Bachelor Project

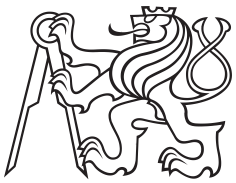

Czech
Technical
University
in Prague

F3

Faculty of Electrical Engineering
Department of Cybernetics

Radioactive regions detection

Jan Charvát

Supervisor: Ing. Vladimír Smutný, Ph.D.
Supervisor–specialist: Ing. Daniel Seifert, Ph.D.
Field of study: Cybernetics and Robotics
Subfield: Robotics
May 2017

Czech Technical University in Prague
Faculty of Electrical Engineering

Department of Cybernetics

BACHELOR PROJECT ASSIGNMENT

Student: Jan C h a r v á t

Study programme: Cybernetics and Robotics

Specialisation: Robotics

Title of Bachelor Project: Radioactive Regions Detection

Guidelines:

1. Get familiar with the problem of radioactive waste sorting.
2. Analyze the radioactive properties of radioactive waste.
3. Analyze the properties of radioactivity detectors in relationship to chosen radioactive waste.
4. Recommend the arrangement of the system for detection of hot-spots in the radioactive waste.
5. Make conclusions.

Bibliography/Sources:

[1] V. Majer a kol.: Základy užité jaderné chemie. SNTL Praha, 1985.
[2] https://www.remm.nlm.gov/civilian.htm
[3] J. Doležal, J. Šťastný, J. Špetlík, S. Bouček: Jaderné a klasické elektrárny - 1. odborná učebnice pro VŠ obor energetika, 2011, http://www.mpo-efekt.cz/uploads/7799f3fd595eeee1fa66875530f33e8a/cvut-1-elektrarny.pdf

Bachelor Project Supervisor: Ing. Vladimír Smutný, Ph.D.

Valid until: the end of the summer semester of academic year 2017/2018

L.S.

prof. Dr. Ing. Jan Kybic
Head of Department

prof. Ing. Pavel Ripka, CSc.
Dean

Prague, January 10, 2017

Acknowledgements

I would like to thank Ing. Vladimír Smutný Ph.D. for his support and his advice throughout this difficult project.

I am also grateful to Ing. Daniel Seifert Ph.D. for his advice and for sharing his practical experience.

Declaration

I declare that the presented work was developed independently and that I have listed all sources of information used within it in accordance with the methodical instructions for observing the ethical principles in the preparation of university theses.

Prague, date .....

.....
signature

Abstract

In this bachelor thesis, which is a part of the project RadioRoSo, we examine and analyze waste from Magnox power plants. These power plants were mostly situated in the Great Britain and they were operated between 1956 and 2015. The analyzed waste mainly consists of pieces of Magnox alloy AL80. Springs from alloy Nimonic 80A are also present in the waste and they are considered to be highly radioactive. A main source of the radiation inside the springs is decay of ^{60}Co, ^{59}Ni, and ^{63}Ni. The other radiation comes from surface contamination. The waste is stored under water. This thesis contains a list of particle detectors. We will take a closer look at NaI(Tl) scintillation detector. There will also be introduced semiconductor, scintillation, and ionization detectors. In the end, we will simulate an output of a single NaI(Tl) detector. This detector will be situated over the pieces of magnox, while the discussed springs will lay inside it. Simulations will rather be illustrative because of inaccurate information about the waste.

Keywords: Radioactive waste, radioactivity, cobalt-60, swarf, magnox

Supervisor: Ing. Vladimír Smutný, Ph.D.

Abstrakt

V této bakalářské práci, která je součástí projektu RadioRoSo, se věnujeme analýze odpadu z Magnoxových jaderných elektráren. Tyto elektrárny se nacházely především ve Velké Británii a byly provozovány v letech 1956 až 2015. Analyzovaný odpad se skládá především z kusů slitiny Magnox AL80. Dále v něm můžeme nalézt pružinky ze slitiny Nimonic 80A, které vykazují zvýšené úrovně radiace. Hlavním zdrojem radiace v pružinkách je rozpad ^{60}Co, ^{59}Ni a ^{63}Ni. Další druhy přítomné radiace jsou spojené s povrchovou kontaminací. Odpad je skladován pod vodou. Práce obsahuje výčet některých detektorů ionizujícího záření. Zaměříme zvláště na scintilační detektor NaI(Tl). Probrány budou ovšem i polovodičové, scintilační a ionizační detektory. Na závěr budeme simulovat výstup jednoho NaI(Tl) scintilačního detektoru. Tento detektor se bude nacházet nad kusy magnoxu, ve kterých budou ležet výše zmíněné pružinky. Simulace budou spíše ilustrativní z důvodu nepřesných informací o odpadu.

Klíčová slova: Radioaktivní odpad, radioaktivita, kobalt-60, swarf, magnox

Překlad názvu: Detekce radioaktivních oblastí

Contents

Figures

Tables

Chapter 1

Introduction

In the year of 1956, the first Magnox power station began to produce electricity. Another 10 power stations were built and started operations by 1971 in Great Britain. A total number of reactors used in those power plants is 26. Two more Magnox power plants were built in Europe outside of the Great Britain. One of those power stations was constructed in Italy, while the other one was built in Japan. Last Magnox power plant in Europe has shut down by the end of 2015 [1].

Magnox power plants also produce plutonium which can be later used in weapon industry. After World War II it was believed that gas-cooled power reactors were the best type for producing plutonium [1].

Magnox reactor is a type of nuclear reactor which uses natural uranium in metallic form as fuel. Natural uranium is made of ^{238}U (99.27 %), ^{235}U (0.72 %) and ^{234}U (0.0056 %). The fuel is in the form of rods which are then contained in a casing made out of magnox. Rods with casing are called fuel element. The power plants were constructed by different companies. It caused some changes in the design of the fuel elements. Magnox reactors were designed so it would be possible to change fuel rods without shutting down the reactor itself [1].

The reactor uses graphite as a moderator. The cooling system uses carbon dioxide as a heat exchange coolant. Carbon dioxide circulates between reactor core, steam generators, and gas circulators [1].

When the fuel in the fuel elements has burned out then fuel rods are taken out of the reactor. The fuel elements are then put under water to die out. After several years the fuel and magnox casing must be separated. The process is called desplittering. Desplittering operations began in 1969. The product of the desplittering is burn-up fuel and fuel element debris (FED).

This work is a part of the project called Radioactive Robotic Sorter (RadioRoSo). Main goal of this project is to demonstrate separation springs

from swarf. Swarf is waste which consists of mainly magnox, Nimonic springs, thermocouples, water and a tiny amount of used fuel. Ideally, no fuel will be present, but the possibility of fuel being present should not be overlooked. An objective of this work is to analyze situation and pick the most suitable radiation detectors which can detect the presence of the Nimonic spring in swarf.

Part I

Situation

Currently, magnox is stored in water after desplittering. Crane picks up about 30 kg of swarf and moves it on trays. The swarf is spread to a few cm thick layer. A tray is about 1 m long and wide [2]. There is a possibility of changing some of these parameters. For example, thickness of the layer will probably be lower to achieve better visibility of the springs.

At the moment, Nimonic springs are being separated by manually controlled manipulators. This process is highly ineffective because workers have to manually operate manipulator to pick up all the springs. They also do not have the detectors to verify if the magnox is free of springs. Therefore, the only way to eliminate the possibility of overlooking spring is to go through the whole pile of the swarf carefully [2].

Waste is divided into 3 types based on activity of the components:

- Low level waste - LLW
- Intermediate level waste - ILW
- High level waste - HLW

LLW is a waste which does not belong to other types. Radioactivity of LLW can vary from just above the background levels in nature to several units of GBq per tonne. LLW is ordinarily produced by hospitals, universities, and others. Some magnox can be classified as an LLW [3].

ILW has higher radioactivity than LLW, but this waste cannot generate sufficient amount of heat to require active cooling. In our case, ILW is represented by Nimonic springs and some magnox [3].

HLW is waste which generates significant heat thanks to its high radioactivity. HLW consists of spent nuclear fuel and byproducts from its reprocessing. There should not be any HLW present in our case but it is possible there will be a very low quantity of spent fuel in form of shreds [3].

For this chapter it is important to have a basic knowledge about neutron activation, β-decay, γ-decay, and electron capture. Neutron activation is a process in which atomic nuclei capture a neutron, several neutrons, and a few other processes which will not be discuses here. The neutrons increase nucleon number by the same amount of the neutrons that were captured. The atom changes into different nuclide. Some created nuclides are stable and some are unstable [4].

Unstable nuclides can undergo these processes: α-decay, β-decay (β^+, β^-, and electron capture), and γ-decay. There are other processes which can occur but we will not discuss them for the sake of simplicity. Generally α-decay is more common in nuclides with a high nucleon number. β^--decay is typical for nuclides where a number of neutrons exceeds a number of protons [5]. β^--decay looks like this:

$$^{\mathrm{A}}_{\mathrm{Z}}\mathrm{X} \rightarrow ^{\mathrm{A}}_{\mathrm{Z+1}}\mathrm{Y} + \mathrm{e}^- + \overline{\nu}_{\mathrm{e}}, \tag{1.1}$$

where X is the unstable element (mother), Y is the daughter element (stable or unstable), A is nucleon number, Z is proton number, e^- is electron and $\overline{\nu}_e$ is antineutrino. Proton-rich unstable atoms can decay via two modes. First mode is electron capture. It is a process where proton-rich nucleus take in electron from electron cloud:

$$ {}^{\mathrm{A}}_{\mathrm{Z}}\mathrm{X} + \mathrm{e}^- \rightarrow {}^{\mathrm{A}}_{\mathrm{Z}-1}\mathrm{Y} + \nu_{\mathrm{e}}, \tag{1.2} $$

where ν_e is neutrino.

Second mode of decay is β^+-decay:

$$ {}^{\mathrm{A}}_{\mathrm{Z}}\mathrm{X} \rightarrow {}^{\mathrm{A}}_{\mathrm{Z}-1}\mathrm{Y} + \mathrm{e}^+ + \nu_{\mathrm{e}}, \tag{1.3} $$

where e^+ is positron [6].

Positron is an antiparticle of electron. When the positron collides with electron, a annihilation occurs. The annihilation is accompanied by emission of two photons (γ-particles) with energy of 0.511 MeV each. This will cause an energy peak at this energy when the photons are measured by a detector [6].

Excess energy after decay of an atom is usually emitted via photons. This process can be called γ-decay when the emitted photon have high energy.

Spectrum of the measured energies will not be discrete but continuous. This is caused by Compton effect as photons may transfer only a portion of their energies into a detector. Some of the photons will leave detector with lower energy. Probability of capture increases as the energy of a photon decreases [7].

Chapter 2

Magnox

Swarf consists mainly of magnox (some sources states even 99.5 % of the weight is magnox alloy). The size of individual pieces is approximately 2 mm x 25 mm x (75-900) mm. Upper weight limit is about 100 g [8].

Magnox is a widely used description for several types of alloys which mostly consists of magnesium. Magnox alloy was used as a cladding for fuel rods. A composition of the magnox alloy AL80 is 0.8 % of aluminium, 0.004 % of beryllium and the rest is magnesium [9].

The most radioactivity of the magnox comes from the surface contamination.

Magnesium in magnox undergoes a chemical reaction with water which creates magnesium hydroxide [10]. Therefore, magnox cannot be stored under water for extended periods of time. One way to deal with magnox waste is to dissolve it in weak carbonic acid. The main advantage of this method is a great reduction of volume (even more than 90 % [11]). Another way is to separate springs, put them in shielded small containers. The containers are placed it in the middle of a big container and surrounded with magnox[2].

2.1 Magnesium

We believe it is safe to assume that the magnesium in magnox have the same percentages as a naturally occurring magnesium because no other information indicates otherwise. Naturally occurring magnesium is formed by three stable nuclides: ^{24}Mg (78.99 %), ^{25}Mg (10 %) and ^{26}Mg (11.01 %) [5]. Neutron activation increases nucleon number by 1. For example when neutron is

captured by ^{24}Mg the product is ^{25}Mg. This reaction can be written as a formula:

$$^{24}\mathrm{Mg} +^{1} \mathrm{n} \rightarrow^{25} \mathrm{Mg}. \tag{2.1}$$

^{25}Mg is stable nuclide therefore no other radioactive decay occurs. ^{25}Mg can also capture neutron which changes this nuclide into the ^{26}Mg which is also stable. More interesting behavior can be observed when neutron is captured by ^{26}Mg:

$$^{26}\mathrm{Mg} +^{1} \mathrm{n} \rightarrow^{27} \mathrm{Mg}. \tag{2.2}$$

^{27}Mg is unstable with a half-life of 9.46 minutes. ^{27}Mg then decays into the ^{27}Al which is again a stable nuclide so the decay will no longer continue [5]:

$$^{27}\mathrm{Mg} \rightarrow {}^{27}\mathrm{Al} + \beta^{-} + \overline{\nu}_{\mathrm{e}}. \tag{2.3}$$

The decay scheme can be seen in the figure 2.1. From previous analysis, it is apparent that even activated magnesium cannot be a significant source of the radiation.

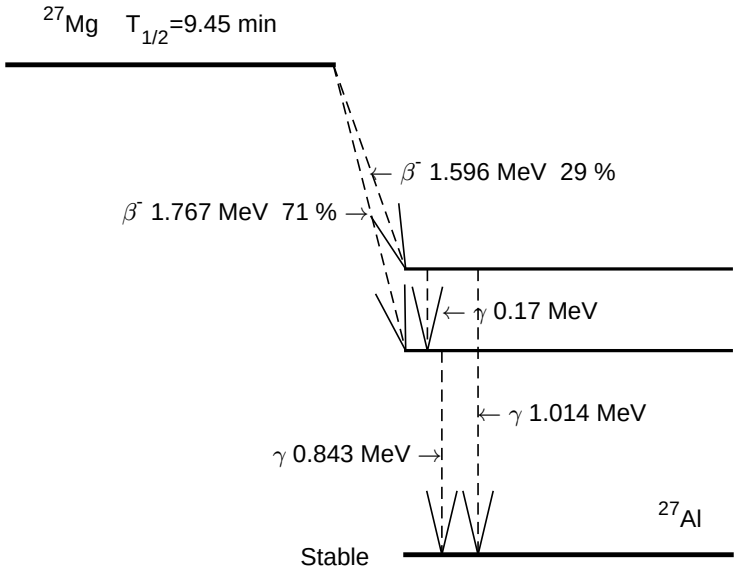

Figure 2.1: Decay scheme of ^{27}Mg

2.2 Aluminium

Let us continue with the analysis of the aluminum. Natural aluminum consists of only one nuclide ^{27}Al. When neutron capture occurs then ^{27}Al becomes

^{28}Al. ^{28}Al is an unstable nuclide with a half-life of 2.24 minutes:

$$^{28}\mathrm{Al} \rightarrow {}^{28}\mathrm{Si} + \beta^{-} + \overline{\nu}_{\mathrm{e}}. \tag{2.4}$$

^{28}Si is a stable nuclide [5]. The decay scheme can be seen in the figure 2.2. As stated before the decay will no longer continue. Aluminum cannot be a significant source of radiation either.

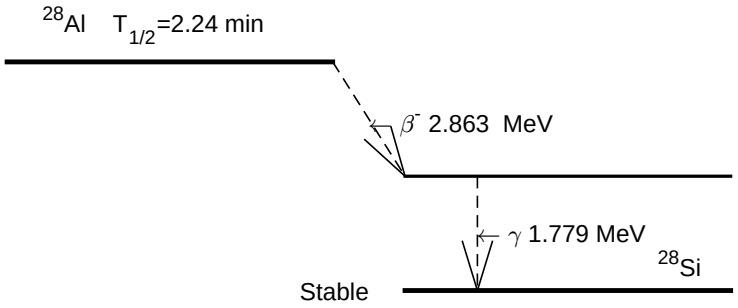

Figure 2.2: Decay scheme of ^{28}Al

2.3 Beryllium

Beryllium has very low concentration in magnox. Only ^{9}Be is stable nuclide hence it is the only nuclide found in nature (except for minor traces). In case of neutron capture ^{9}Be changes to ^{10}Be. ^{10}Be is not stable but decays into the ^{10}B. Half-life of the ^{10}Be is $1.39 \cdot 10^{6}$ years [5]. ^{10}Be undergoes this decay:

$$^{10}\mathrm{Be} \rightarrow {}^{10}\mathrm{B} + \beta^{-} + \overline{\nu}_{e}. \tag{2.5}$$

Decay scheme is in the figure 2.3. Beryllium has a long half-life thus can and will be the source of radiation in magnox. Beryllium has a low concentration and a long half-life which causes its a lower activity. The activity of ^{10}Be is not important because only β^{-}-particle is emitted. It is easily attenuated by the material itself or a thin layer of metal.

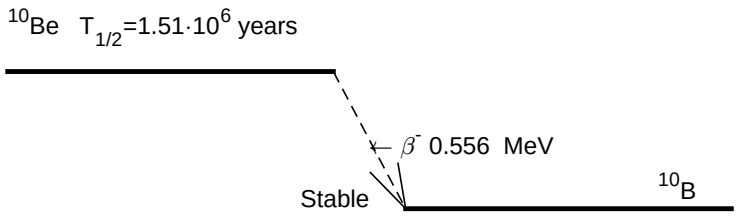

Figure 2.3: Decay scheme of ^{10}Be

2.4 Summary

In magnox, only beryllium will undergo radioactive decay. Other elements have an inferior half-life in comparison to the time that the waste had spent in storage. Most of the radioactivity comes from surface contamination. In this case, we will assume that surface contamination will be the same as surface contamination of the springs.

Chapter 3

Springs

The goal of RadioRoSo project is demonstration of the spring separation from the swarf. The springs are used at the top ending where spider a spring-arm is. The spider spring-arm has two uses. In the first place, it centres fuel element inside a fuel channel. In the second place, the spring inside reduces vibrations produced by the gas flow [1].

These springs are about 33 mm long and 10 mm in diameter [12]. The wire used for the production of these springs is said to be about 1 mm in diameter [2]. Approximate weight of one spring is about 5 g. They are made of Nimonic alloy 80A which is an alloy of nickel, chrome, titanium and aluminum [13]:

- Ni: balance
- Cr: 18-21 %
- Ti: 1.8-2.7 %
- Al: 1-1.8 %
- Fe: max 3 %
- Co: max 2 %
- Mn: max 1 %
- Si: max 1 %
- Other elements: max 0.5 %

Further analysis will ignore aluminum because it was addressed in the previous chapter.

3.1 Nickel

Nickel is found in nature in form of ^{58}Ni (68.08 %), ^{60}Ni (26.22 %), ^{61}Ni (1.14 %), ^{62}Ni (3.63 %), and ^{64}Ni (0.93 %). ^{58}Ni is the most common nuclide of nickel so let us begin there. ^{58}Ni will change into ^{59}Ni after capturing a neutron. ^{59}Ni is unstable nuclide with half-life of about $7.6 \cdot 10^4$ years. ^{59}Ni undergoes electron capture where this nuclide changes into ^{59}Co [5]. There is no γ-particle emission as you can see in the figure 3.1.

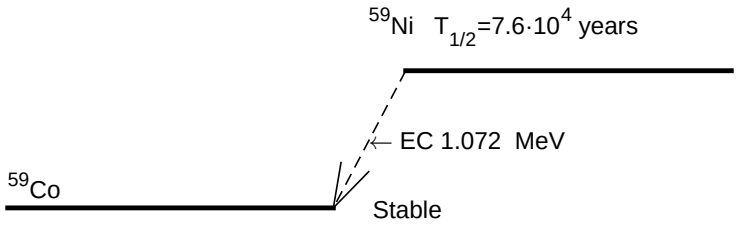

Figure 3.1: Decay scheme of ^{59}Ni

Next nuclide of nickel which can create unstable nuclide is ^{62}Ni. This nuclide becomes ^{63}Ni after capturing a neutron. ^{63}Ni has a half-life of 100.1 years [5]. Decay can be seen in a figure 3.2 and it can be written as:

$$^{63}\text{Ni} \rightarrow {}^{63}\text{Cu} + \beta^- + \overline{\nu}_e. \tag{3.1}$$

The energy of the β^--particle can be as high as 67 keV. ^{63}Cu is a stable nuclide. No γ-radiation is present in this decay [5].

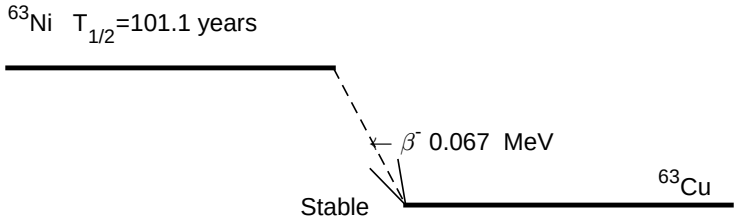

Figure 3.2: Decay scheme of ^{63}Ni

^{63}Ni has the highest activity alongside with ^{59}Ni. β^--particle can be stopped by a few millimeters of aluminum. Large portion of emitted β^--particles is also absorbed inside the radioactive material itself. In our case it is

possible for a spring to be in between pieces of magnox. Detecting β-particles would be less reliable than detecting high penetrable γ-particles.

Last relevant nuclide of nickel is ^{64}Ni. When exposed to neutron flux, some atoms of this nuclide changes into ^{65}Ni which undergoes a radioactive decay. ^{65}Ni has a half-life of 2.52 hours [5]. It decays into stable ^{65}Cu. Different β^--particles can be emitted as you can see in the figure 3.3. The activity of ^{65}Ni is negligible in contrast with a time spend in storage.

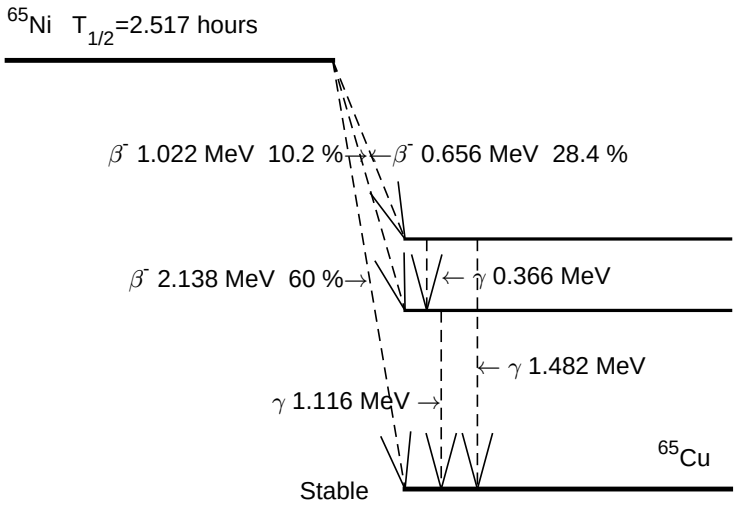

Figure 3.3: Decay scheme of ^{65}Ni

3.2 Chromium

A Nimonic alloy consists of chromium of about (18-21 %). In nature, chromium appears in a form of 3 stable and one observationally stable nuclide. These are: ^{50}Cr (4.3 %), ^{52}Cr (83.8 %), ^{53}Cr (9.5 %), and ^{54}Cr (2.4 %). There will be mainly 2 unstable nuclides created after inserting the chromium into a neutron flux. These are ^{51}Cr and ^{55}Cr. ^{51}Cr decays by two possible ways into a stable nuclide ^{51}V. The half-life of ^{54}Cr is 27.7 days. The first possibility of decay is via electron capture. The probability of only electron capture occurring is about 90.6 % [5]. Other possibility is an electron capture with an emission of excess energy in a form of γ-particle with energy of about 320 keV. Graphical interpretation of this decay can be seen in the figure 3.4 [5].

^{55}Cr decays into the ^{55}Mn. ^{55}Cr has a half-life of about 3.5 minutes. As stated before, nuclides with this short half-life will not be present in the springs. The decay is shown in the figure 3.5.

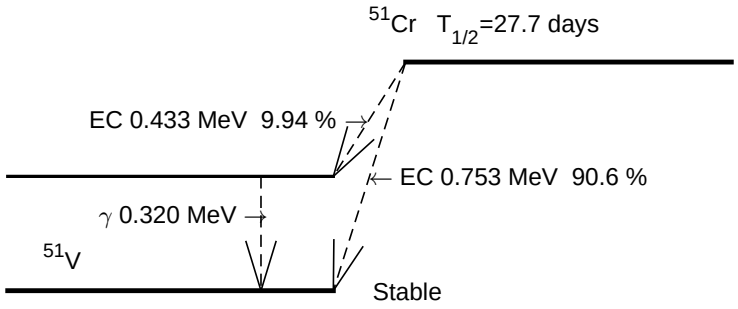

Figure 3.4: Decay scheme of ^{51}Cr

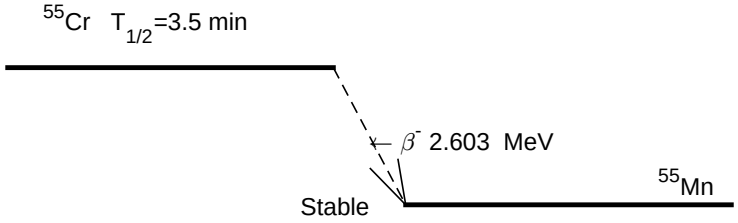

Figure 3.5: Decay scheme of ^{55}Cr

3.3 Titanium

Titanium can be found in nature in a form of 5 nuclides: from ^{46}Ti through ^{48}Ti (73.7 %) to ^{50}Ti. Just like in other cases, only nuclides created by one neutron absorption will be considered. ^{51}Ti is the only nuclide worth analyzing. ^{51}Ti decays into the ^{51}V. As stated before ^{51}V is a stable nuclide. ^{51}Ti has a half-life of 5.76 minutes [5]. Titanium contained in springs is not a source of radioactivity because of the short half-life. Decay scheme is shown in the figure 3.6.

3.4 Iron

Iron comes in many forms. In our case in the form of many nuclides. We will briefly introduce stable ones, but more important are, of course, unstable nuclides.

^{54}Fe is observationally stable and by absorbing neutron it becomes ^{55}Fe. ^{55}Fe has a half-life of 2.737 years and decays via electron capture into stable ^{55}Mn [5]. After several decades of storage ^{55}Fe will still have some remaining

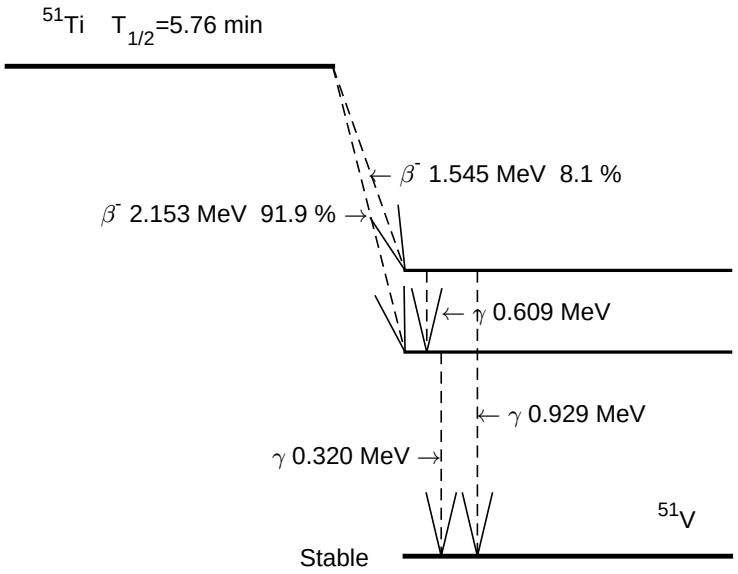

Figure 3.6: Decay scheme of ^{51}Ti

activity. Figure 3.7 shows decay scheme of ^{55}Fe.

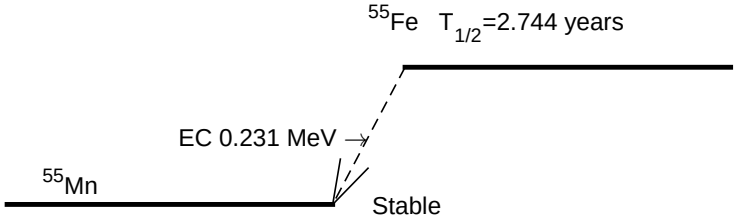

Figure 3.7: Decay scheme of ^{55}Fe

Stable nuclides of iron are ^{56}Fe (91.75 %), ^{57}Fe (2.12 %), and ^{58}Fe (0.28 %). Only one of these three is relevant to us. It is the ^{58}Fe. ^{58}Fe will change into an unstable ^{59}Fe after neutron capture. ^{59}Fe is unstable nuclide with a half-life of about 44.5 days. ^{59}Fe is likely to decay via electron capture into a stable ^{59}Co [5]. It is shown in the figure 3.8.

3.5 Cobalt

Only one stable nuclide of cobalt exists. It is ^{59}Co. ^{59}Co will form ^{60}Co after it has been activated by a neutron. ^{60}Co has the half-life of 5.27 years. ^{60}Co can decay via two scenarios. First and most probable scenario (99.88 %) is an

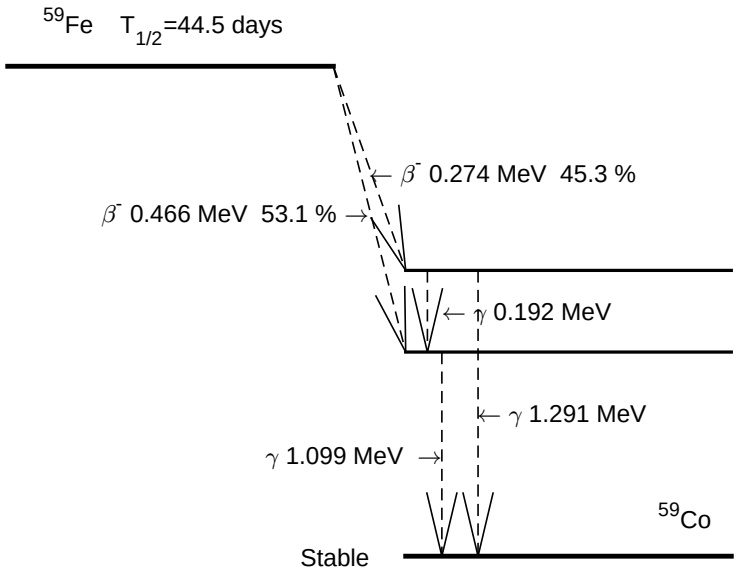

Figure 3.8: Decay scheme of ^{59}Fe

emission of β^--particle with energy up to 317.05 keV followed by 2 emissions of γ-particles with energies 1.17 MeV and 1.33 MeV respectively. The other outcome of this decay is the emission of β-particle with energy of up to 1.48 MeV followed by γ-particle with energy of 1.33 MeV similarly to the previous decay mode [5]. This decay is shown in the figure 3.9.

^{60}Co is one of the three nuclides which are responsible for most of the radioactivity produced by springs. ^{60}Co has, in our case, another first rank. It emits more γ-rays than any other nuclide in springs. As stated before, ^{59}Ni and ^{63}Ni only emit β^--particles.

3.6 Manganese

Only one stable manganese nuclide exists. It is ^{55}Mn. ^{55}Mn increases its nucleon number via neutron capture and changes into the ^{56}Mn. ^{56}Mn is an unstable nuclide with a half-life of 2.58 hours. ^{56}Mn decays into a stable ^{56}Fe via β^--decay. There exist several variant of this decay [5]. It can be seen in the figure 3.10. Activated manganese cannot be a source of the radioactivity in the springs because of its short half-life.

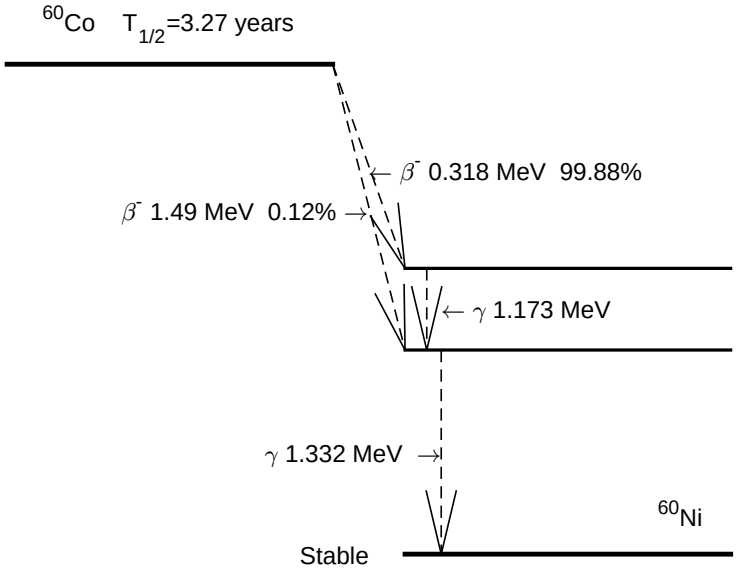

Figure 3.9: Decay scheme of ^{60}Co

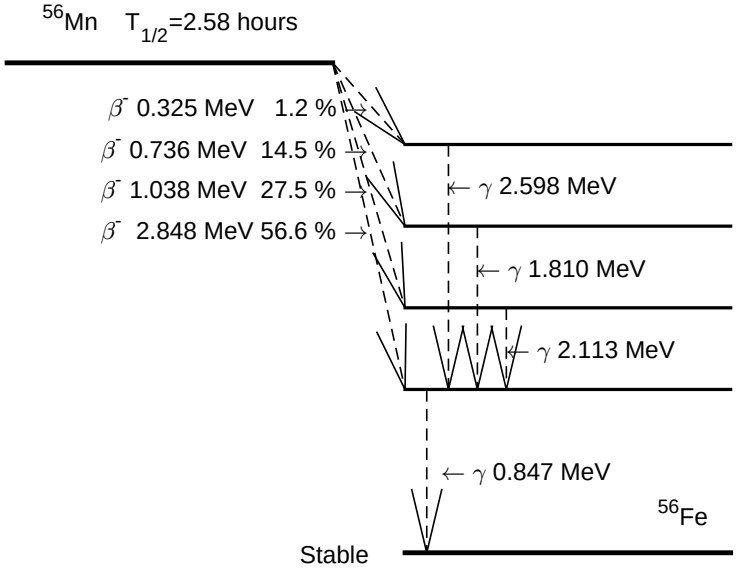

Figure 3.10: Decay scheme of ^{56}Mn

3.7 Silicon

Stable silicon nuclides are ^{28}Si (92.2 %), ^{29}Si (4.7 %), and ^{30}Si (3.1 %). After neutron activation ^{31}Si can be created. It has a half-life of 157.36 minutes [5]. The figure 3.11 shows this decay scheme. After storage, the amount of ^{31}Si will be insignificant.

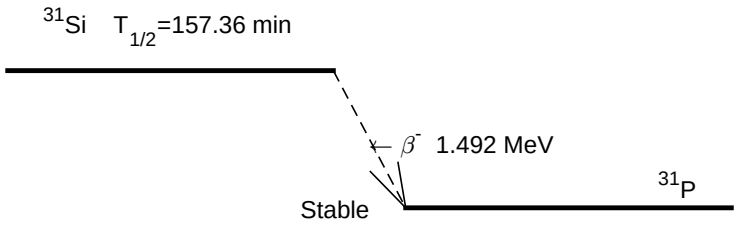

Figure 3.11: Decay scheme of ^{31}Si

3.8 Spring activity calculation

Now that we know which nuclides are significant, it would be convenient to find out the activity of a single spring. The storage time of the springs may vary significantly. As stated above, magnox power plants in Europe have been in operation from 1956 to 2015. This brings a possibility of two extreme cases. Some of the springs may be stored for over 60 years while many other may be stored for a couple of years. They were also positioned at a different places in the reactor which means neutron flux was not the same. Different waste streams have different activity. Another problem is an uncertainty in the activity of the waste streams. As you can see, we cannot determine the activity of a single spring. However, acquiring this information is essential for simulation. We will assume the springs in the waste stream will have the same activity even if that is not true. The calculation will be done using data from waste from power plant Dungeness A [14].

In this analysis we will take a closer look at ^{60}Co, ^{59}Ni, and ^{63}Ni. Mean radioactivity is estimated with uncertainty of a factor 10. The activity in the waste stream were calculated for 1.4.2016 [14]. We do not have more specific information available.

One spring weights about $m = 5g = 5 \cdot 10^{-3}kg$. The density of separated springs (about 90 %) and thermocouples (rest of the volume) is roughly $\rho = 1.5 \cdot 10^{3}kg/m^{3}$. Activity of ^{60}Co is about $A_{^{60}Co} = 1.53 \cdot 10^{13}Bq/m^{3}$. Next

calculation illustrates how to obtain mean activity of a single spring:

$$A_{s^{60}Co} = \frac{A_{60Co} \cdot m}{\rho} = \frac{1.53 \cdot 10^{13} \cdot 5 \cdot 10^{-3}}{1.5 \cdot 10^{3}} = 51\text{MBq}, \tag{3.2}$$

where $A_{s^{60}Co}$ is the activity of ^{60}Co in a single spring in April 2016. We will update activities to 1.5.2017 by this equation:

$$A^{2017}_{s^{60}Co} = A_{s^{60}Co} e^{-\frac{ln(2)\cdot t}{T_{1/2}}} = 51 \cdot 10^{6} e^{-\frac{0.693 \cdot 1.082}{5.272}} = 44.2\text{MBq}, \tag{3.3}$$

where t is time difference between $A_{s^{60}Co}$ and $A^{2017}_{s^{60}Co}$ - $t = 1.082$ years, $T_{1/2}$ is half-life of ^{60}Co. The mean activity $A^{2017}_{s^{60}Co}$ of one spring is about 44.2 MBq.

We have information about several other waste streams from different power plants. There are about 10 % of thermocouples mixed in a waste stream from Dungeness A. Other calculations were created similarly to the previous example. Results can be seen in the table 3.1.

Waste		9C47 [14]	9D39 [15]	9D43 [16]
Site		Dungeness A	Hinkley Point	Hinkley Point
ρ	[kg/m^3]	1.5	0.82	0.82
$A_{^{60}Co}$	[TBq/m^3]	15.3	175	105
$A^{2017}_{s^{60}Co}$	[MBq]	44.2	926	555
$A_{^{59}Ni}$	[TBq/m^3]	10	10	10
$A^{2017}_{s^{59}Ni}$	[MBq]	33.3	61	61
$A_{^{63}Ni}$	[TBq/m^3]	946	1890	10
$A^{2017}_{s^{63}Ni}$	[MBq]	50.6	1059	636
Waste		9E40 [17]	9E43 [18]	9G40 [19]
Site		Oldbury	Oldbury	Trawsfynydd
ρ	[kg/m^3]	1.5	1.5	1.5
$A_{^{60}Co}$	[TBq/m^3]	31.8	162	13.6
$A^{2017}_{s^{60}Co}$	[MBq]	91.9	393	39.3
$A_{^{59}Ni}$	[TBq/m^3]	10	10	10
$A^{2017}_{s^{59}Ni}$	[MBq]	33.3	33.3	33.3
$A_{^{63}Ni}$	[TBq/m^3]	959	1920	959
$A^{2017}_{s^{63}Ni}$	[MBq]	105	450	45

Table 3.1: Counted activity of a spring from different sources

We can anticipate springs with lower average activity at the beginning of project RadioRoSo. Other waste will stay stored in the mean time. Their activity will, therefore, decrease. The most significant drop can be expected in activity of ^{60}Co. On the other hand nuclides of nickel will keep similar activity.

Chapter 4

Surface contamination

Surface contamination is present, because the swarf is stored underwater. Fuel rods from fuel elements can also leave some dust in the process of desplittering. Big number of radionuclides is present. In this analysis, we will take a closer look at some of the more important ones. The importance will be decided at the threshold of $10^8 Bq/m^3$ in mean activity. Data will be collected from several waste streams.

The first radionuclide is ^{3}H also known as tritium or T. Tritium will most likely be present in a form of tritiated water - T_2O. T decay via β^--decay. No photon is emitted in this process, therefore, ^3H is not relevant for future measurement [5].

Next nuclides with sufficient activities are ^{14}C, ^{36}Cl and ^{90}Sr. All of them decay via emitting β^--particle without generating any γ-particles [5].

^{113m}Cd is a meta state of ^{113}Cd. It undergoes β^--decay without emission of γ-particles [5].

^{115m}Sn is also a meta state of a nuclide. ^{115m}Sn can emit high number of low energy photons. All of these photons have energies under 40 keV [5].

^{133}Ba is a nuclide, which undergoes a decay via electron capture. In this process, several γ-particles are also emitted. There are a few possibilities. Let us take into consideration only the most probable ones. The energy of these γ-particles is 0.356 MeV (34 %), 0.302 MeV (32.9 %), and 0.081 MeV (32.9 %) [5].

^{137}Cs decays via β^--decay. In this process, γ-particle is emitted (85.1 %). It has an energy of 0.662 MeV. Detection of high amount γ-particles with this energy indicates that some fraction of the fuel is present in the measured swarf. ^{137}Cs is main source of surface contamination. We will consider radiation from ^{137}Cs as a background [5].

^{147}Pm decays via β^--decay. It is possible for this nuclide to emit photons, however, it is very unlikely (under 0.005 %) [5].

^{241}Pu mostly undergoes β^--decay. Probability of emission γ-rays is very low (under 10^{-5} %) [5].

4.1 Background activity calculation

We will consider the sources of radiation from magnox and from surface contamination as a background activity. Just like everything else, uncertainty of the activities is factor of 10. The calculation will not take the effect of the α and β particles into consideration, because they will be attenuated by lead shielding.

As stated before, the only measurable radionuclide contained in magnox is ^{10}Be. The activity of this nuclide is several times lower than the activity from surface contamination. Most of the generated γ-particles will be produced by ^{133}Ba and ^{137}Cs.

The trays are about 1 meter long and wide. Waste will be loaded on top of these. The idea is to spread the waste into thin layer. Thickness of this layer could be up to 25 mm. Total volume of waste on the tray is $V = 1$ m·1 m·2.5 cm= 0.025 m^3. The density is around $\rho = 280\ kg/m^3$. The calculations will be done similarly to spring activity calculation:

$$A_{total^{137}Cs} = A_{^{137}Cs} \cdot V = 1.63 \cdot 10^8 \cdot 2.5 \cdot 10^{-2} = 4.075\text{MBq}. \tag{4.1}$$

$A^{2017}_{total^{137}Cs}$ means activity of the whole tray with $V \cdot \rho$ kg of swarf from ^{137}Cs in May 2017.

$$A^{2017}_{total^{137}Cs} = V \cdot A_{^{137}Cs} \cdot \mathrm{e}^{-\frac{t*ln2}{T_{1/2}}}, \tag{4.2}$$

where $t = 1.082s$ (which is about 395 days), $T_{1/2}$ is half-life of ^{137}Cs. Results can be seen in the table 4.1.

Activities differ very much. This can be caused by several reasons. The first of them is differing time spent in storage. Another reason is, that the surface contamination depends on how much dust and how many pieces of fuel are there in the storage within the swarf.

Waste stream		9B25 [20]	9B57 [21]	9A43 [22]
Site		Bradwell	Bradwell	Berkeley
ρ	$[kg/m^3]$	280	280	570
$A_{^{133}Ba}$	$[MBq/m^3]$	<135	<158	<111
$A^{2017}_{total^{133}Ba}$	$[MBq]$	3.2	3.7	2.63
$A_{^{137}Cs}$	$[MBq/m^3]$	39.6	55.5	56.8
$A^{2017}_{total^{137}Cs}$	$[MBq]$	0.97	1.35	1.39
Waste stream		9J23 [23]	9C24 [24]	9E24 [25]
Site		Hunterston A	Dungeness A	Oldbury
ρ	$[kg/m^3]$	250	700	350
$A_{^{133}Ba}$	$[MBq/m^3]$	<33.7	<111	<0.404
$A^{2017}_{total^{133}Ba}$	$[MBq]$	0.8	2.63	0.01
$A_{^{137}Cs}$	$[MBq/m^3]$	610	163	261
$A^{2017}_{total^{137}Cs}$	$[MBq]$	14.87	3.97	6.36

Table 4.1: Counted activities of the magnox on one tray from different sites

Part II

Detectors

Chapter 5

Ionization detector

Ionization detectors are detectors designed to produce electric output based on a number of ion pairs created in a medium. Ion pair is a pair consisting of an ion and a free electron. It is generated by incident particle colliding with a molecule in the medium. An ion and electron would recombine almost immediately. Such recombination is, however, undesirable because the event has not been measured yet. To prevent this from happening an electric field is applied to the medium [26].

Ionization detectors usually use chamber filled with gas. The design of the chamber may vary a lot. The chamber contains two electrodes - anode and cathode. High voltage is applied to electrodes which generate the electric field. The ions are pulled towards cathode and the electrons are pulled towards anode where they can be measured as a charge or electrical current [26].

There is a possibility to create one side of the chamber out of glass for measuring α and β particles. This will provide lower attenuation coefficient so fewer particles will be stopped by the chasing of the chamber. This design also improves sensitivity in one direction. In our case, detection of α and β particles will not be used [26].

Magnitude of voltage determines how the chamber works as you can see at figure 5.1. The regions are:

- I. Ohm region
- II. Ionization region
- IIIA. Proportional region
- IIIB. Geiger region

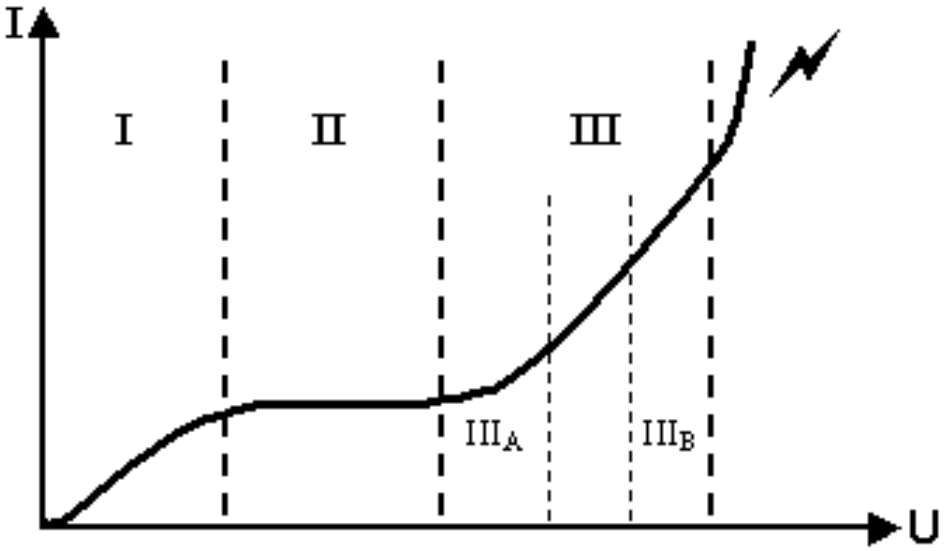

Figure 5.1: "Volt-ampere characteristic" of ionization chamber [27]

Ion and electrons recombine in Ohm region. Therefore, this region is not used for detection.

5.1 Ionization region

Ionization counter works in ionization region. When ionization particle hits a molecule of gas inside the chamber it generates an ion pair. The electric charge created by one ion pair is very low, therefore, there must either be high incident radiation for producing more ion pairs or there must be applied low-noise amplifier before measuring its charge [28].

The voltage is high enough to prevent ion pair recombination. The voltage is yet low enough to prevent secondary ion pair production.

We can distinguish two types of ionization counters:

- Pulse type
- Current type.

Pulse type ionization counter produces voltage pulses via quick collection of electrons. Current type ionization counter produce direct current which can

be measured or amplified [28].

Ionization counter can be used for measuring energy of the incident particle. The reason behind this is that the number of created ion pairs correspond to the original energy of the particle without being amplified inside the chamber [26]. This type of detector is not suitable for our application as we need to detect high-energy γ-particles which would mostly go through the chamber undetected.

5.2 Proportional region

A proportional counter works in proportional region. The proportional counter is similar to the ionization chamber. In this case, voltage between electrodes is higher than threshold voltage needed for producing secondary ion pairs (voltage belongs to the proportional region). It means that electrons produced by ionization are accelerated towards the anode. These electrons have a higher speed, therefore, are able to create a secondary ion pair when they collide with another molecule. This way ion pairs multiply, therefore, charge is amplified. Consequently even sources with lower activity which emit lower energy can be detected without the need to use the low-noise amplifier as in the ionization counter [26].

The proportional counter is capable of measuring the energy of an incident particle but with lower resolution than an ionization chamber. However, it is not suitable for our application as we need to detect high-energy γ-particles which would mostly go through the chamber undetected.

5.3 Geiger region

Geiger counter works in Geiger-Müller region. Applied voltage is higher than the voltage used in proportional counter. The ions achieve a higher speed when they are pulled towards the anode, therefore, they are able to ionize more molecules. This causes an avalanche effect. In theory, the avalanche effect causes almost full ionization in the chamber after collision of a gas molecule with the particle of our interest. All impulses have the same magnitude because full ionization occurs after roughly the same amount of avalanches. After the gas has been fully ionized there are almost no molecules which could produce more electrons after the collision with ionization particle [29].

Geiger counter counts a number of impulses generated by full ionization of the chamber. An important parameter of Geiger counter is dead time. Almost fully ionized chamber does not create another avalanche even if some other

ionization particle creates an ion pair. Therefore, chamber must recombine into initial state in order to create another avalanche. Dead time is a time period needed for the chamber to recombine. Dead time can be as long as 1 ms [26].

Geiger counter can also be used for detection of high energy γ-particles. Geiger counter needs ionization of a single molecule in order to create an impulse. When a γ-particle collides with matter in the detector's wall, an electron is emitted. The electron may fly into the chamber itself and create a secondary ion pair. This way the avalanche is triggered and an impulse can be detected. The electron may also be absorbed by the material of the wall. This creates a limit on the thickness of the wall. If the wall is thicker than maximum range of the electron, then the rest of the wall works only as a shielding [29].

Geiger counter could be potentially used but there are better detector for our application.

Chapter 6

Scintillation detector

Scintillation detectors usually consist of a scintillator, a photomultiplier tube, and a photodetector.

The scintillator is a material which converts the energy of ionization particle into measurable light. If the energy of ionization particle is smaller than ionization energy, then molecule or atom which has been hit will become excited. De-excitation of an atom or a molecule is accompanied by emitting a photon. This photon can be amplified and eventually measured [26].

One ionization particle can cause more atoms or molecules to become excited, therefore, more photons are emitted.

When the photon is emitted it can be absorbed by scintillator itself. To prevent it from happening scintillators should have very low attenuation coefficient for the wavelength of the generated photon [26].

Scintillators can be divided into two groups:

- Organic scintillators
- Inorganic scintillators.

Photomultiplier tube is glass tube in which there is photocathode, few dynodes, and anode. There is a vacuum inside the tube. Final multiplication of the tube depends on the number of used dynodes, number of generated photons and other parameters. Multiplication can vary in the range of about $10^4 - 10^7$ [26].

6.1 Organic scintillators

Organic scintillators can be divided into several groups [29]:

- Pure organic crystals
- Liquid organic solutions
- Plastic scintillators

6.1.1 Pure organic crystals

Mainly used scintillators in this category are anthracene and stilbene. One difficulty surrounding anthracene and stilbene is their production. Also, both of them are fragile. Scintillation efficiency of anthracene is bigger than any other organic scintillator [29]. As they cannot be produced in large sizes, these detectors are not suitable for our task.

6.1.2 Liquid organic solutions

Liquid scintillators can be obtained by dissolving an organic scintillator. There can also be another material added to work as a wavelength shifter if needed. Liquid scintillators can be mixed with a sample of radioactive material. This method is used for measuring particles with a low energy [29]. There is no reason to pick this detector. High activity can be expected in our application.

6.1.3 Plastic scintillators

Plastic scintillators can be created in a variety of forms and sizes. It is one of the main advantages of plastic scintillators. There is a wide selection of commercially available types and shapes. The material of scintillators varies according to measured particle so its efficiency would be the best.

Plastic scintillators have lower service life due to the damage caused by

radiation to the fluorescent component or due to the creation of absorption areas inside scintillators [29]. These detectors could be used in the project RadioRoSo, however, there are more suitable types.

6.2 Inorganic scintillators

Main advantages of inorganic scintillators over organic ones is longer life time. On the other side inorganic scintillators have lower decay times (around $10^{-6}s$ opposed to $10^{-8}s$ with organic ones) [26]. For measuring high energy γ-rays sodium iodide scintillator is often used.

6.2.1 Sodium iodide

Sodium iodide (NaI(Tl)) scintillator is a thallium-activated sodium iodide crystal. When a high-energy photon reacts with sodium it creates electron-hole pair. Freed electron can then excite thallium. De-exciitation of thallium emits a photon in the visible spectrum (around 415 nm). NaI(Tl) is often used for measuring activities of ^{60}Co. Their efficiency is highly dependent on the quality of the crystal [29].

Sodium iodide can grow into large crystals. Several cubic centimeters is not an exception. The larger the crystal the higher efficiency it can achieve. For example the company Saint-Gobain Ceramics & Plastics, Inc. offers crystal of size 10 cm x 10 cm x 100 cm [30].

NaI(Tl) is hygroscopic. It means that crystals must be somehow isolated from water and moisture. NaI(Tl) crystals are usually sealed in a metal casing [29].

NaI(Tl) works well in room temperature. It is better for the crystal not to work in rapid temperature changing environment. Otherwise the crystal can shatter. The crystals of NaI(Tl) are also very fragile.

Creation of the electron-hole pair needs about 20 eV of energy. One γ-particle with energy of 1 MeV creates up to 38 000 photons with average energy about 3 eV [29][26].

In case we would want to measure the energy of the particle, then I suggest using this type of the sensor for measuring. Decay of the ^{60}Co emits two photons with an energy of 1.17 MeV and 1.33 MeV. This sensor is conventionally used for detection of previously mentioned photons. Price of this sensor is also lower than of some other choices and it does not require cooling.

Chapter 7

Semiconductor detector

Semiconductor detectors are somewhat similar to ionization detectors. In this case, when an incident ionization particle collides with a molecule of the semiconductor, the electron-hole pair is created (as opposed to electron-ion pair in ionization detectors). The energy needed is low (Silicon and germanium require about 3.5 eV) [26]. It means for every absorbed 3.5 eV one electron-hole pair will be created. The energy needed for creation of an electron-ion pair in ionization chambers, is about 10 times higher [31]. Semiconductor detector is, therefore, more accurate in terms of measuring energy.

One way to use semiconductor detectors is by using a semiconductor as the p-n reversed-biased diode. When the diode is connected to voltage, then the area between p-type and n-type is depleted. When an incident ionization particle interacts with matter, it creates an electron-hole pair. The electron is then pulled towards the n-type and the hole is "pulled" towards the p-type. This creates a current pulse which can be detected by a serially connected resistor. Created pulse is proportional to the energy of the ionization particle [31].

For accurate measurement, a voltmeter must have low noise.

The material used as semiconductor may vary from silicone, germanium, through diamond to cadmium telluride (or cadmium zinc telluride). Every material has its advantages and disadvantages.

Cadmium telluride (CdTe) and cadmium zinc telluride (CdZnTe) is used as a material for detection of hard γ-rays. It is because its high nucleon number and high density.

7.1 Germanium semiconductor detectors

The major problem of using germanium is its leakage currents. The semiconductor have to be cooled to lower the impact on measurements. Liquid nitrogen is usually used in order to bring the temperature down to about 77 K [32]. Another disadvantage is a relatively low nucleon number of germanium which lowers the probability of a gamma-ray interaction. For these reasons this detector is not as good as other ones.

7.2 Silicone semiconductor detectors

Silicone detectors also suffer from a low nucleon number. These detectors can operate at room temperature but they are more often than not cooled by liquid nitrogen. Lower temperature limits the effect of leakage currents. Silicone detectors degrade more rapidly than other semiconductor detectors. There are, however, other ways to decrease degrade rate. For all these reasons the detector is not suitable for this project.

7.3 Cadmium (zinc) telluride semiconductor detectors

The main advantage of CdTe and CdZnTe semiconductor detectors lies within its high nucleon number. Thanks to this property the detectors have high efficiency of high energy γ-particles detection. Both of these detectors are commercially available in a thick or a thin form. The thin form has a lower probability of stopping high energy photons. In our case we need to detect photons with energies above 1 MeV which means we need to use the thick form [33].

CdTe compound suffers from time instability when electrical field is applied. Instability comes from polarization effect and it causes lowering charge collection and counting rate. There are possibilities to decrease the impact of polarization. For example lowering temperature or increasing applied electrical field can solve this problem to some extent [33].

Adding small portion of zinc into the material increases its resistivity which lowers leakage currents. For comparison, resistivity of CdTe is about $10^9 \Omega cm$ while CdZnTe has resistivity of about $10^{10} \Omega cm$. This effectively decreases

leakage currents by a factor of 10. CdZnTe does not suffer from polarization like CdTe [33].

CdTe and CdZnTe semiconductor detectors are suitable for our case. The only downside is their higher price. NaI(Tl) can achieve the same efficiency because it can be much larger.

Part III

Simulations

Chapter 8

Arrangement of detectors

Swarf can be very radioactive. Measured activities will vary a lot because of random number of the springs on the tray and various extinction time periods. The activity may be up to dozens of TBqm^{-3} [21][22].

Now the situation and types of detectors have been introduced, let us take a look at position and arrangement of detectors. Many ideas have been discussed regarding the topic of detectors at the initial meeting [2]. The arrangement of detectors depends on the type that will be used. The arrangements are:

- Single detector
- Line of the detectors
- Matrix of detectors
- Manipulator equipped with the detector
- Detectors under the tray
- γ-camera attached to the ceiling

Some of the arrangements can return estimated position of the spring. However, the manipulator also needs azimuth and elevation of the spring. The optical camera will be used in every scenario to obtain such information.

Some sort of a collimator is recommend to ensure low interference from sources outside of the tray. One of those sources can be for example a gripper

used by the manipulator. Gripper will accommodate surface contamination after the process. The room itself might also be contaminated by dust from the swarf.

8.1 Single detector

In this instance, every detector mentioned earlier can be used. Result of the measurement will be either "There are no longer any springs" or "there are some springs left". The number of springs cannot be obtained because of uncertainties in their activity. Rough estimation can be made only when the springs would have similar activities and the detector would be calibrated.

8.2 Line of the detectors

Approximate position of the spring can received by tray moving under the line of the detectors. Imagine a scenario where an optical camera determines there are no more springs. Let us consider that some pieces of magnox lay on top of a spring. The tray will move under the line to determine whether or not the tray is spring free. In this scenario the detectors would roughly specify the area where the spring lays. The manipulator could move around in waste to spread the pieces of magnox. Camera might then be able to find the overlooked springs. Basically every type of detector can be used. The only limitation is the cost of the detectors.

Another kind of set-up is worth mentioning. The line of detectors can move instead of the trays. This method is more complicated because another engine is needed for movement of the detectors. Main advantage opposed to moving tray is that the next tray can be sorted out while this one is being measured. Silicon and germanium semiconductors cannot be used for this method because they require cooling by liquid carbon dioxide. It is possible to connect pipes into moving structure, however, it is unnecessarily complicated.

The time of measurement would increase opposed to a single detector. The measurement needs to be done several times over the tray so complete information would be available. Also, adding more detectors means increasing price.

8.3 Matrix of detectors

The only way this setup could be used is by fixing the matrix outside of the manipulation area of the robot. Trays need to move under the matrix and stay still for a while in order to get the measurement. This case is most time-effective as the tray is measured whole at once. The matrix will likely be placed closer to the tray than the set-up with a single detector. Every detector has to cover smaller area. We want to obtain the estimated position of the spring. Ideally, the spring in front of one detector would not be detected by other detectors. Time of exposure would be either shorter or the same as using a single detector.

The number of detectors may rise in order to increase resolution. A downside of this approach is a high number of detectors, therefore a high price. Theoretically, every type of detector can be used. Practically, the Geiger counter is the only type cheap enough to be used in high number.

8.4 Manipulator equipped with the detector

Manipulator can be equipped with a single detector. This way the detector can move to any spot. Measurements can be interpolated to find the most probable position of the spring. When the spring is not visible the manipulator can move to several spots eventually moving closer to the spring. This method works well when single spring is not visible but in case of several hidden springs this method might take long time. Also another manipulator is more expensive than adding more detectors. This idea is presented because the original idea was to use two manipulators. This set-up is worse than other methods in many ways, therefore, it is not worth recommending.

8.5 γ-camera attached to the ceiling

γ-camera is capable of finding exact location of the spring. Accuracy of the information, depends on the type of the γ-camera and time of measurement. Even if γ-camera accurately locates the spring, the manipulator will still need to know azimuth and elevation of the spring. γ-camera is also very expensive. This arrangement is also not worth recommending.

8.6 Summary

From previous analysis it is not apparent which method is the most suitable. It is a single detector. NaI(Tl) scintillation detector is ideal for this application because from its output it is possible to distinguish the energy of photons. We can expect high number of photons with low energy from the surface contamination. It is also possible to use CdZnTe but the price of the detector is higher than NaI(Tl).

Chapter 9

Simulations

Simulations use point sources for the springs. In the chapter about situation, there is a statement about crane picking up about 30 kg of swarf. However, this part will most likely change for our own sake. The trays will probably contain single layer of the swarf.

Precise information about activity of the spring and magnox is not available. For this reason, it would be best to choose one of the sites, where we have information about both springs and magnox. Data from streams 9C24 [24] and 9C47 [14] will be used for the simulation. Both streams come from power plant Dungeness A.

9.1 Calculation

The goal of these calculations is to determine how many γ-particles will be absorbed by the material of the detector. It depends on the density and the thickness of the material as well as on the energy of the γ-particle. Photons can interact with matter via several mechanics, therefore, it is better to take into consideration the intensity of photons rather than interaction of a single one. Number of captured photons I can be calculated by this equation:

$$I = I_0(1 - \mathrm{e}^{-\frac{\mu_m l}{\rho}}), \tag{9.1}$$

where I_0 is the number of incident photons, μ_m is the mass attenuation coefficient, l is the thickness of the material and ρ is the density of the material. For convenience μ_m can be subsidized by a linear attenuation

coefficient μ:

$$\mu = \frac{\mu_m}{\rho}. \tag{9.2}$$

Final equation is:

$$I = I_0(1 - \mathrm{e}^{-\mu l}). \tag{9.3}$$

μ and μ_m can be obtained from tables and graphs.

9.2 Geometry

I_0 depends on the geometry. Let us imagine a situation where the source is one point. When the distance between the detector and the source is much bigger than the size of the detector. Then I_0 can be calculated as:

$$I_0 = I_s \frac{S_d}{4\pi r^2}, \tag{9.4}$$

where I_s is the number of emitted photons from source, r is the distance between the source and the detector. S_d is the projection of the area of the detector into a sphere around the source with radius r.

In our case, the previous assumptions could not be. It is caused by the size of the detector and its distance from the tray. One way to deal with this problem is to calculate S_d and make very complex function to find out the thickness of the material at each point on S_d. This function would depend on the shape of the detector.

For following simulations the detector is replaced by cuboid with same l and S_d. The cuboid is then divided into M^2 elements and for each of these elements l and S_d is calculated. At this point $I_{i,j}$ can be calculated, where $I_{i,j}$ is number of photons captured by the i,j-th element. I can be found by this equation:

$$I = \sum_{i=1}^{M} \sum_{j=1}^{M} I_{i,j}. \tag{9.5}$$

At first, we need to find which vertex of the cuboid is the closest to the source. $\overrightarrow{v}$ is the vector from source to the vertex. Then we need to know the vectors of all three edges, which connects to the vertex. Each of these edges is then divided into smaller parts. Let's say we separate the edges into M fragments. The number of elements will then be M^2. Let us find out how big is the projected area $S_{i,j}$ of the i,j-th element ($i, j \in < 1, M-1 >$). $\overrightarrow{u_i}$ represents vector from the source to the i-th fraction of the edge. The projected area $S_{i,j}$ can be calculated as:

$$S_{i,j} = \| \, (\overrightarrow{u_{i+1}} - \overrightarrow{u_i}) \times (\overrightarrow{u_{j+1}} - \overrightarrow{u_j}) \, \| \, . \tag{9.6}$$

Now we need to find $\overrightarrow{r_{i,j}}$, which is a vector pointing from the source to the center of the area $S_{i,j}$. It can be found like this:

$$\overrightarrow{r_{i,j}} = 0.5(\overrightarrow{u_i} + \overrightarrow{u_{i+1}} + \overrightarrow{u_j} + \overrightarrow{u_{j+1}}) - \overrightarrow{v}. \tag{9.7}$$

The number of captured photons which come through one side can be calculated as:

$$I = \sum_{i=1}^{M-1} \sum_{j=1}^{M-1} I_s \frac{S_{i,j}}{4\pi r_{i,j}^2}. \tag{9.8}$$

We suppose use of the shielding with pin-hole collimator. Therefore, only one side of the detector will be exposed.

9.3 Dose rate

Some sources of particles are more dangerous than other. Dose rate can be used as an indicator of a presence of the spring.

The dose rate is measured in Grey per second or Gy/s. Grey is defined as the absorption of one joule of radiation energy per kilogram of matter. The dose rate Dr of γ-particles can be calculated as:

$$Dr = \frac{\mathrm{d}D}{\mathrm{d}t}, \tag{9.9}$$

where D is absorbed dose [34]. Absorbed dose of γ-particles is calculated as:

$$D = I_0 \Delta t \frac{1 - \mathrm{e}^{-\mu l}}{V\rho} E_\gamma, \tag{9.10}$$

where I_0 is number of incident particles per second, μ is a linear attenuation coefficient, l is a thickness of the material, V is a volume of the material, ρ is a density of the material, and E_γ is an energy of the particles [34]. We assume that the particles have the same energy and the density is constant over the material. We can substitute absorbed dose from equation (9.10) into equation (9.9). The dose rate Dr can be calculated as:

$$Dr = I_0 \frac{1 - \mathrm{e}^{-\mu l}}{V\rho} E_\gamma. \tag{9.11}$$

Let us apply this calculation for a single element mentioned in previous section. This way we obtain formula for calculation of element dose rate $Dr_{i,j}$ which is being absorbed in i,j-th element:

$$Dr_{i,j} = I_s \frac{S_{i,j}(1 - \mathrm{e}^{-\mu l_{i,j}})}{4\pi r_{i,j}^2} \frac{E_\gamma}{V_{i,j}\rho}. \tag{9.12}$$

Volume of i, j-th element $V_{i,j}$ is the only information we do not have. We can, however, calculate it. In the figure 9.1 shows approximation of the i, j-th element. S_b is area of the base of the pyramid and $l_{i,j} + r_{i,j}$ is a height of the pyramid with base S_b.

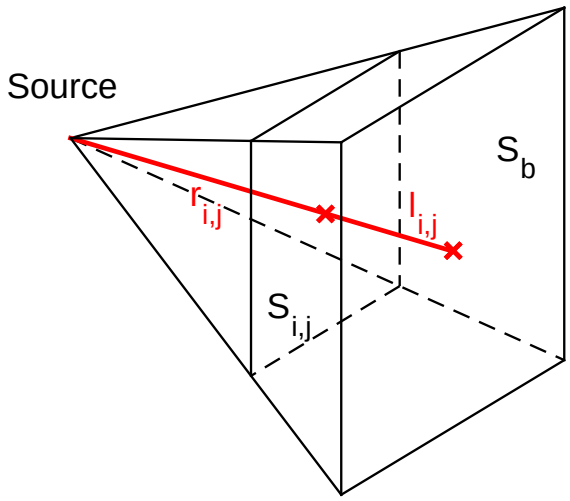

Figure 9.1: Approximation of element i, j used for numerical integration.

Volume $V_{i,j}$ can be calculated as:

$$V_{i,j} = \frac{1}{3}(S_b(r_{i,j} + l_{i,j}) - S_{i,j}r_{i,j}). \tag{9.13}$$

Again we do not know base area S_b. Because of a similarity of triangles we can write:

$$\frac{\sqrt{S_b}}{r_{i,j} + l_{i,j}} = \frac{\sqrt{S_{i,j}}}{r_{i,j}}, \tag{9.14}$$

where $\sqrt{S_b}$ is length of sides of the base. Now we can substitute S_b from equation (9.14) into equation (9.13). Then we can substitute$V_{i,j}$ into equation (9.12). Finally we have solution where all parameters are known:

$$Dr_{i,j} = I_s \frac{S_{i,j}}{4\pi r_{i,j}^2} \frac{E_\gamma}{\rho} \frac{3r_{i,j}^2}{S_{i,j}((r_{i,j} + l_{i,j})^3 - r_{i,j}^3)} = I_s \frac{3E_\gamma}{4\pi\rho((r_{i,j} + l_{i,j})^3 - r_{i,j}^3)}. \tag{9.15}$$

Dose rate of photons with energy E_γ will be calculated as:

$$Dr = \sum_{i=1}^{M-1} \sum_{j=1}^{M-1} I_s \frac{3E_\gamma}{4\pi\rho((r_{i,j} + l_{i,j})^3 - r_{i,j}^3)}. \tag{9.16}$$

These calculations have to be done for every photon with different energy. Total dose rate is a sum of all dose rates calculated for different energy of photons.

9.4 Background

As a background activity we will consider the sources of radiation from magnox and from surface contamination. In reality background activity is defined as a activity without the presence of any spring. Just like everything else, uncertainty of the activity is a factor of 10. The calculation will not take into consideration the effect of α and β particles, because they will be attenuated by magnox itself and a thin layer of metal chasing of the detector.

As stated in the previous chapter, the only radionuclide contained in magnox is ^{10}Be. Activity of this nuclide are several times lower than the activity of surface contamination. The most of the generated γ-particles will be produced by ^{133}Ba and ^{137}Cs. Background activity are approximated by 25 point sources spread equally across the tray.

The spring will be approximated by a single source. The presence of the spring can be judged by detecting photons generated by ^{60}Co.

$\mu_{NaI(Tl)}$ is linear attenuation coefficient of the NaI(Tl). NaI(Tl) is a compound of mainly two elements - Sodium iodide. Linear attenuation coefficient of NaI for photons with energy of 1.17 MeV can be calculated as [35]:

$$\mu_{\mathrm{NaI}}^{1.17} = \frac{\mathrm{M_{Na}}}{\mathrm{M_{NaI}}}\mu_{\mathrm{Na}}^{1.17} + \frac{\mathrm{M_I}}{\mathrm{M_{NaI}}}\mu_{\mathrm{I}}^{1.17}, \tag{9.17}$$

where $\mu_{\mathrm{Na}}^{1.17}$ is linear attenuation coefficient of sodium for photons with energy of 1.17 MeV and $\mathrm{M_{Na}}$ is molar mass of sodium. Other symbols are created similarly. Other linear attenuation coefficients can be seen in the table 9.1.

Source	probability	energy [MeV]	$\mu_{NaI(Tl)}$ $[cm^{-1}]$	μ_{Pb} $[cm^{-1}]$
^{133}Ba	34 %	0.081	5.73	44.62
^{133}Ba	32.9 %	0.302	0.17	4.57
^{133}Ba	62 %	0.356	0.077	3.6
^{137}Cs	85.1 %	0.662	0.0.079	1.31
^{60}Co	99.88%	1.17	0.054	0.74
^{60}Co	100%	1.33	0.05	0.65

Table 9.1: Linear attenuation coefficients for photons generated by background [35]

9.5 Shielding

We want to detect particles which come only from the tray. We have to assume that a room, where the process of separation will happen, will become contaminated by dust from the swarf. We will need to use shielding so the contamination will influence the measurement only a tiny bit. It can be achieved by putting the detector into a lead well. The well looks like a tube which has one side almost completely closed except for a window, where the detector is placed. A collimator will also be used. The collimator prevents detection of the particles that comes from anywhere except for the tray.

Lead is commonly used for shielding. Another materials that can be used are tungsten and iron. Tungsten is more expensive but it has better properties. It has a higher nucleon number and higher density. Therefore, it is more likely to absorb high energy γ-particles. Iron has worse properties so thicker layer must be used for shielding. We will most probably use lead well.

On the table 9.2 you can see linear attenuation coefficients of lead, iron and a tungsten alloy W* (W (90 %), Ni (6 %) and Cu (4 %)).

energy [MeV]	μ_{Pb} $[cm^{-1}]$	μ_{W*} $[cm^{-1}]$	μ_{Fe} $[cm^{-1}]$
1	0.77	1.08	0.56
0.5	1.7	2.14	1.27
0.2	10.6	11.5	7.79
0.1	60.4	64.8	43.69

Table 9.2: Linear attenuation coefficients of lead (Pb), tungsten alloy (W*) and iron (Fe) [36]

Chapter 10

Results of simulations

10.1 Single NaI(Tl) detector

In this section we will take a closer look into this arrangement. The activity of the background is 2.63 MBq for ^{133}Ba and 3.97 MBq for ^{137}Cs. The background activity were calculated from waste stream 9C24 [24] from Dungeness A. The waste is evenly distributed over 1 m x 1 m tray with thickness of 25 mm. This distribution is approximated by 25 sources evenly spread around the tray.

NaI(Tl) is used as a scintillation detector. Parameters of photomultiplier tube will be ignored for the sake of simplicity. NaI(Tl) has a diameter of 51 mm and a height of 51 mm.

First we will simulate detection of background. It is a situation where spring is not present. It can be seen in the figure 10.1.

Now we will add a spring. The spring is situated in the middle of the tray right under the detector. Let us assume that this position has coordinates [50,50,0]. The activity of ^{60}Co is 44.2 MBq. It is calculated from waste stream 9C47 [14] from site Dungeness A.

Spring in the middle of the tray is the easiest to detect. The worst position where spring can lay is in the corner of the tray. The position can be written as [0,0,0]. Counts per second highly depend on the position of the spring as you can see in the figures 10.2 and 10.3. The difference is almost a factor of 10.

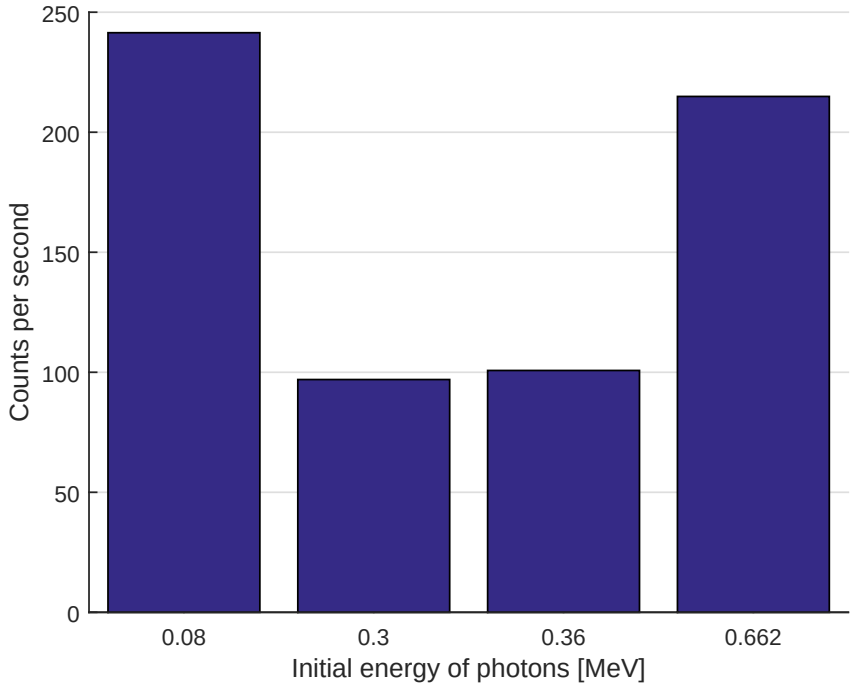

Figure 10.1: Counts per second by a detector without any springs.

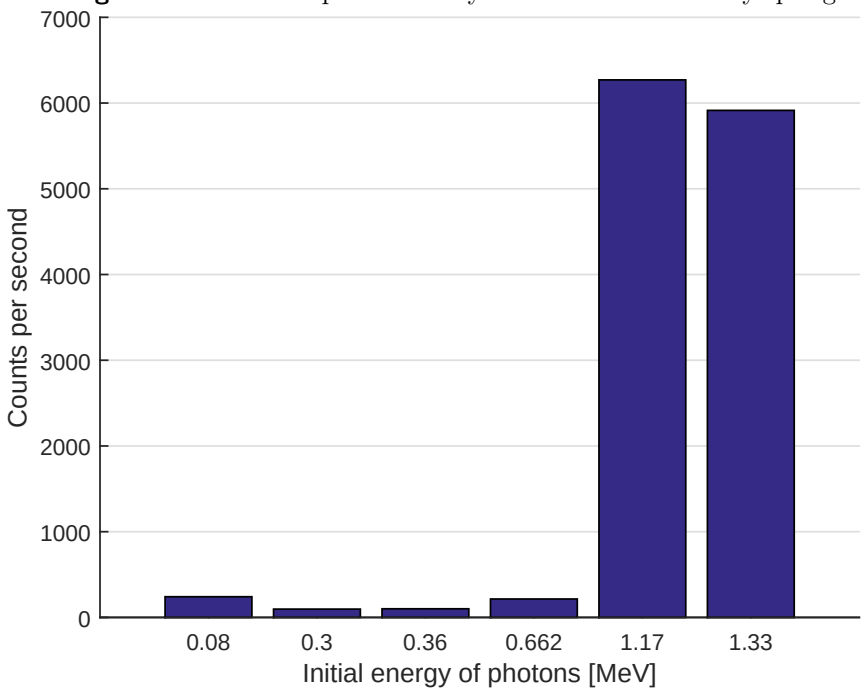

Figure 10.2: Counts per second with spring situated in the middle of the tray.

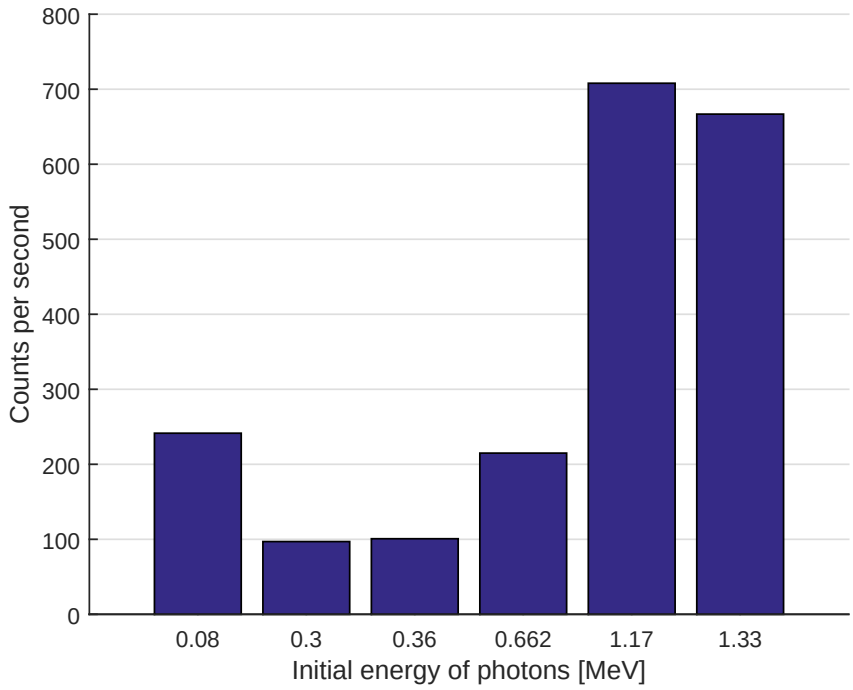

Figure 10.3: Counts per second with spring situated in the corner of the tray.

We can identify the energy which the particle lost inside the detector, therefore, we can calculate dose rate. As you can see in the figures 10.4 and 10.5 the dose rate from the background is much smaller than dose rate from a single spring. The separation of the spring is used for decreasing dose rate from the waste. If the waste would exhibit high activity when no spring would be present then it may not be ideal to mix this waste together with some other. This way we can detect such waste and some other process may occur. For example the waste may be washed to lower surface contamination. For these reasons we suggest measuring dose rate instead of count rate.

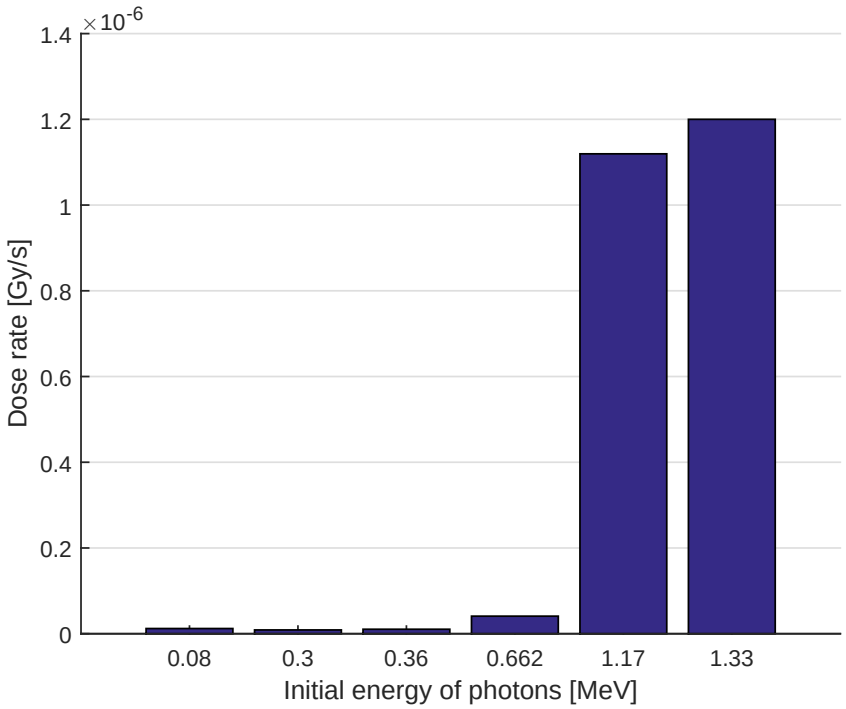

Figure 10.4: Detected dose rate with spring situated in the middle of the tray.

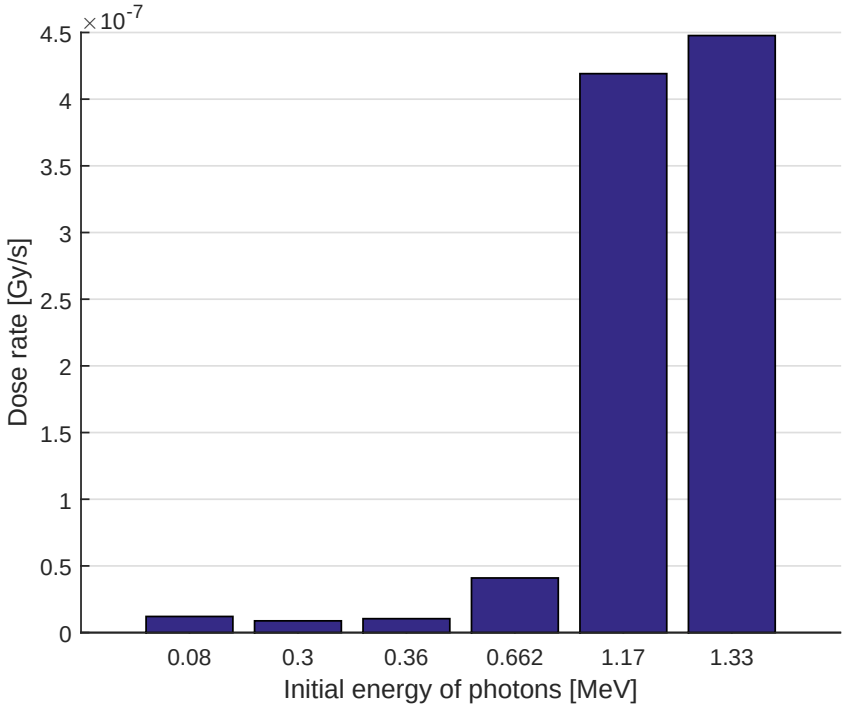

Figure 10.5: Detected dose rate with spring situated in the corner of the tray.

Chapter 11

Conclusion

The goal of this thesis is to analyze the waste and to suggest appropriate detectors alongside with their arrangement. The analysis of waste has been done by analyzing wastes from other nuclear power plants. It is not the most precise calculation because of the uncertainty of the radioactivity of the waste. Because we do not posses more accurate information, the final arrangement of detectors could be a bit different. The easiest parameters to change is the threshold. Calibration of the detectors will have to be done manually at least once.

The analysis found that most activity of the springs comes from ^{63}Ni and ^{59}Ni. These nuclides, however, do not emit any γ-particles. They are hard to detect because the emitted particles are absorbed by magnox which can lay over the springs. Most of β-particles is also absorbed in the spring itself. ^{60}Co is also present in the springs. This nuclide usually emits two γ-particles with energies 1.17 MeV and 1.33 MeV. These two γ-particles are harder to detect because of their high energy. However, detection of these photons is needed in order to determine the presence of a spring.

The most important nuclides in the rest of the swarf are ^{137}Cs and ^{133}Ba. Both of these come from surface contamination. In the process of decay of ^{137}Cs γ-particle with energy 0.662 MeV is likely to be emitted. The energy of this γ-particle is also relatively high in contrast with other γ-particles present.

As for the detectors, I suggest using a single NaI(Tl) scintillation detector with a diameter of 51 mm and a height of 51 mm.

NaI(Tl) scintillator can be used to determine energy of the particles. We can filter counts from photons with lower energy. This way we can safely find the springs even with high activity from surface contamination. Another advantage is that we can detect presence of pieces of the fuel. We are, however, not able to find or even pick up the fuel piece so some other process would have to occur.

Radiation dose rate can also be calculated. If the radiation dose rate would be high and no springs nor pieces of fuel would be present then some other process could be used to lower activity. For example the magnox could be washed so the surface contamination would decrease. I suggest using dose rate detection over count rate detection.

Precision of the calculations in the simulation were under 10 % for count rate. These calculations were unnecessarily complex because of the uncertainty of the activity is a factor of 10. Similar output could be calculated easier with almost the same precision when we take into consideration the uncertainty of the activity. If the activity would be measured then the simulation might prove to be useful.

Bibliography

[1] JENSEN, S. E, E NONBØL, NORDISK KERNESIKKERHEDSFORSKNING a NORDIC NUCLEAR SAFETY RESEARCH. *Description of the Magnox type of gas cooled reactor (MAGNOX)*. Roskilde: NKS, 1999. ISBN 978-87-7893-050-7.

[2] BASSO, Andrea, personal interview, 1. 11. 2016

[3] UK Radioactive Waste Inventory. *About radioactive waste* [online] Moor Row: UK Radioactive Waste Inventory, 2017. [seen 2017-05-12]. Available from: https://ukinventory.nda.gov.uk/about-radioactive-waste/what-is-radioactivity/what-are-the-main-waste-categories/

[4] ALI M.A., Nuclear Research Center, Atomic Energy Authority. *A Brief Overview of Neutron Activation Analyses Methodology and Application* [online] Cairo, Egypt: 2nd Conference on Nuclear and Particle Physics, 1999. [seen 2017-05-12]. Available from: http://www.iaea.org/inis/collection/NCLCollectionStore/_Public/37/118/37118483.pdf

[5] IAEA - Nuclear Data Section. *Live Chart of Nuclides - nuclear structure and decay data* ms:*2210*.[online] Vienna: IAEA Nuclear Data Section, 2017. [seen 2017-05-12]. Available from: https://www-nds.iaea.org/relnsd/vcharthtml/VChartHTML.html

[6] Ullmann, V. *Radioaktivita*. [online] Ostrava - Poruba: astronuklfyzika.cz. [seen 2017-05-12]. Available from: http://http://astronuklfyzika.cz/JadRadFyzika2.htm

[7] Ullmann, V. *Radioaktivita*. [online] Ostrava - Poruba: astronuklfyzika.cz. [seen 2017-05-12]. Available from: http://http://astronuklfyzika.cz/JadRadFyzika6.htm

[8] UK Radioactive Waste Inventory. W*aste Stream 9E25 FED Magnox* [online] Moor Row: UK Radioactive Waste Inventory, 2016. [seen 2017-05-12]. Available from: https://ukinventory.nda.gov.uk/wp-content/uploads/sites/18/2017/03/9E25.pdf

[9] HIGGINS, G.T. *Secondary recrystallisation in magnox AL 80.* Journal of Nuclear Materials [online]. 1963, 8(2), 153-159 [cit. 2017-05-23]. DOI: 10.1016/0022-3115(63)90030-8. ISSN 00223115. Dostupné z: http://linkinghub.elsevier.com/retrieve/pii/0022311563900308

[10] UK Radioactive Waste Inventory. *Waste Stream 2D24 Magnox Cladding and Miscellaneous Solid Waste* [online] Moor Row: UK Radioactive Waste Inventory, 2016. [seen 2017-05-12]. Available from: https://ukinventory.nda.gov.uk/wp-content/uploads/sites/18/2017/03/2D24.pdf

[11] NDA - Nuclear Decommissioning Authority, Magnox Ltd., Energy Solutions. *Magnox plan summary - Magnox lifetime plan 2013* [online] Berkley: Magnox Ltd., 2013. [seen 2017-05-12]. Available from: http://www.magnoxsites.co.uk/wp-content/uploads/2014/02/Magnox-Plan-Summary-2013.pdf

[12] UK Radioactive Waste Inventory. *Waste Stream 9C24 FED Magnox - Solid Secondary Waste* [online] Moor Row: UK Radioactive Waste Inventory, 2016. [seen 2017-05-12]. Available from: https://ukinventory.nda.gov.uk/wp-content/uploads/sites/18/2017/03/9B79.pdf

[13] BIBUS METALS. *NIMONIC® Alloy 80A*[online] Brno: BIBUS METALS s.r.o., 2017. [seen 2017-05-12]. Available from: http://www.bibusmetals.cz/materialy/nikl-niklove-slitiny/nimonicr-alloys/nimonicr-alloy-80a/

[14] UK Radioactive Waste Inventory. *Waste Stream 9C24 Nimonic Springs and Thermocouples* [online] Moor Row: UK Radioactive Waste Inventory, 2016. [seen 2017-05-12]. Available from: https://ukinventory.nda.gov.uk/wp-content/uploads/sites/18/2017/03/9C47.pdf

[15] UK Radioactive Waste Inventory. *Waste Stream 9C24 FED Nimonic R1* [online] Moor Row: UK Radioactive Waste Inventory, 2016. [seen 2017-05-12]. Available from: https://ukinventory.nda.gov.uk/wp-content/uploads/sites/18/2017/03/9D39.pdf

[16] UK Radioactive Waste Inventory. *Waste Stream 9D43 FED Nimonic - R1* [online] Moor Row: UK Radioactive Waste Inventory, 2016. [seen 2017-05-12]. Available from: https://ukinventory.nda.gov.uk/wp-content/uploads/sites/18/2017/03/9D43.pdf

[17] UK Radioactive Waste Inventory. *Waste Stream 9E40 FED Nimonic* [online] Moor Row: UK Radioactive Waste Inventory, 2016. [seen 2017-05-12]. Available from: https://ukinventory.nda.gov.uk/wp-content/uploads/sites/18/2017/03/9E40.pdf

[18] UK Radioactive Waste Inventory. *Waste Stream 9E43 FED Nimonic [online]* Moor Row: UK Radioactive Waste Inventory, 2016. [seen 2017-05-12]. Available from: https://ukinventory.nda.gov.uk/wp-content/uploads/sites/18/2017/03/9E43.pdf

[19] UK Radioactive Waste Inventory. *Waste Stream 9G40 FED Nimonic* [online] Moor Row: UK Radioactive Waste Inventory, 2016. [seen 2017-05-12]. Available from: https://ukinventory.nda.gov.uk/wp-content/uploads/sites/18/2017/03/9G40.pdf

[20] UK Radioactive Waste Inventory. *Waste Stream 9B25 FED Magnox* [online] Moor Row: UK Radioactive Waste Inventory, 2016. [seen 2017-05-12]. Available from: https://ukinventory.nda.gov.uk/wp-content/uploads/sites/18/2017/03/9B25.pdf

[21] UK Radioactive Waste Inventory. *Waste Stream 9B57 FED Magnox* [online] Moor Row: UK Radioactive Waste Inventory, 2016. [seen 2017-05-12]. Available from: https://ukinventory.nda.gov.uk/wp-content/uploads/sites/18/2017/03/9B57.pdf

[22] UK Radioactive Waste Inventory. *Waste Stream 9A43 FED Magnox* [online] Moor Row: UK Radioactive Waste Inventory, 2016. [seen 2017-05-12]. Available from: https://ukinventory.nda.gov.uk/wp-content/uploads/sites/18/2017/03/9A43.pdf

[23] UK Radioactive Waste Inventory. *Waste Stream 9J23 FED Magnox* [online] Moor Row: UK Radioactive Waste Inventory, 2016. [seen 2017-05-12]. Available from: https://ukinventory.nda.gov.uk/wp-content/uploads/sites/18/2017/03/9J23.pdf

[24] UK Radioactive Waste Inventory. *Waste Stream 9C24 FED Magnox (Lugs)* [online] Moor Row: UK Radioactive Waste Inventory, 2016. [seen 2017-05-12]. Available from: https://ukinventory.nda.gov.uk/wp-content/uploads/sites/18/2017/03/9C24.pdf

[25] UK Radioactive Waste Inventory. *Waste Stream 9E24 FED Magnox* [online] Moor Row: UK Radioactive Waste Inventory, 2016. [seen 2017-05-12]. Available from: https://ukinventory.nda.gov.uk/wp-content/uploads/sites/18/2017/03/9E24.pdf

[26] DAS, A., FERBEL, T. *Introduction to nuclear and particle physics.* 2nd ed. New Jersey: World Scientific, 2009. ISBN 978-981-238-744-8.

[27] Ullmann, V. *Detekce a spektrometrie ionizujícího záření.* [online] Ostrava - Poruba: astronuklfyzika.cz. [seen 2017-05-12]. Available from: http://astronuklfyzika.cz/DetekceSpektrometrie.htm

[28] SECO, J., CLASIE, B., PARTRIDGE, M. Review on the characteristics of radiation detectors for dosimetry and imaging. *Physics in*

Medicine and Biology [online]. 2014, 59(20), R303–R347. [seen 2017-04-24].ISSN 0031-9155, 1361-6560. Available from: doi:10.1088/0031-9155/59/20/R303

[29] KNOLL, G. F. *Radiation detection and measurement.* 3rd ed. New York: John Wiley & Sons Wiley, 2000. ISBN 978-0-471-07338-3.

[30] Saint - Gobain Crystals, *NaI(Tl) and Polyscin® NaI(Tl) Sodium Iodide Scintillation Material* [online] Hiram: Saint-Gobain Ceramics & Plastics, Inc, 2016. [seen 2017-05-12]. Available from: http://www.crystals.saint-gobain.com/sites/imdf.crystals.com/files/documents/sodium-iodide-material-data-sheet.pdf

[31] KAMAL, *A. Nuclear Radiation Detectors.* In: Particle Physics [online]. Berlin, Heidelberg: Springer Berlin Heidelberg, 2014 [seen 2017-05-12], s. 1–78. ISBN 978-3-642-38660-2. Available from: doi:10.1007/978-3-642-38661-9_1

[32] TAKAHASHI, T., WATANABE, S. *Recent progress in CdTe and CdZnTe detectors.* IEEE Transactions on Nuclear Science [online]. 2001, 48(4), 950–959. [seen 2017-05-12]. ISSN 00189499. Available from: doi:10.1109/23.958705

[33] DEL SORDO, S., ABBENE, L., CAROLI, E., MANCINI, A.M., ZAPPETTINI, A., UBERTINI, P. *Progress in the Development of CdTe and CdZnTe Semiconductor Radiation Detectors for Astrophysical and Medical Applications.* Sensors [online]. 2009, 9(5), 3491–3526. [seen 2017-05-12]. ISSN 1424-8220. Available from: doi:10.3390/s90503491

[34] Cremaldi, L. *Basics of Radiation Dosimetry for the Physicist* [online] Mississippi: The University of Mississippi - The Department of Physics and Astronomy, 2016. [seen 2017-05-12]. Available from: `http://www.phy.olemiss.edu/~cremaldi/PHYS415/Basics%20of%20Radiation%20Dosimetry%20for%20the%20Physicist.pdf`

[35] Hubbell J.H., and Seltzer S.M. *Tables of X-ray mass attenuation coefficients and mass energy-absorption coefficients from 1 keV to 20 MeV for elements Z = 1 to 92 and 48 additional substances of dosimetric interest* (version 1.4)[Online], 2004. NIST Physical Reference Data. [seen 2017-04-24]. Available from https://www.nist.gov/pml/x-ray-mass-attenuation-coefficients

[36] Nelson, G., Reilly, G. *Gama-Ray Interactions with Matter.* In: Passive Nondestructive Analysis of Nuclear Materials. Los Amos National Laboratory, NUREG/CR-5550, LA-UR-90-732, 1991, pp. 27-42

Appendix

Waste streams

Information about waste streams are included for convenience. Included ones are:

- 9E25 [8]
- 2D24 [10]
- 9B79 [12]
- 9C47 [14]
- 9D39 [15]
- 9D43 [16]
- 9E40 [17]
- 9E43 [18]
- 9G40 [19]
- 9B25 [20]
- 9B57 [21]
- 9A43 [22]

- 9J23 [23]
- 9C24 [24]
- 9E24 [25]

Simulation software

Simulation program consists of two functions and one script. It was designed on MATLAB 2014b. All generated graphs were created using this software.